Atomic Layer Deposition of Nb-doped ZnO for Thin Film Transistors

A. Shaw[1], J. S. Wrench[2], J. D. Jin[1], T. J. Whittles[3], I. Z. Mitrovic[1], M. Raja[1], V. R. Dhanak[3], P.R. Chalker[2] and S. Hall[1a)]

[1] *Department of Electrical and Electronic Engineering, University of Liverpool, Liverpool, L69 3GJ, United Kingdom*

[2]*School of Engineering, Centre for Materials and Structures, University of Liverpool, Liverpool L69 3GH, United Kingdom*

[3]*Department of Physics and Stephenson Institute of Renewable Energy, University of Liverpool, Liverpool L69 3BX, United Kingdom*

We present physical and electrical characterization of niobium-doped zinc oxide (NbZnO) for thin film transistor (TFT) applications. The NbZnO films were deposited using atomic layer deposition. X-ray diffraction measurements indicate that the crystallinity of the NbZnO films reduces with increasing Nb content and lower deposition temperature. It was confirmed using X-ray photoelectron spectroscopy that Nb^{5+} is present within the NbZnO matrix. Furthermore, photoluminescence indicates that the band gap of the ZnO increases with higher Nb content which is explained by the Burstein-Moss effect. For TFT applications, a growth temperature of 175 ^{o}C for 3.8% NbZnO provided the best TFTs characteristics with saturation mobility 7.9 cm^2/Vs, current On/Off ratio of 1×10^8 and subthreshold swing of 0.34 V/decade. The transport is seen to follow a multiple-trap and release mechanism at lower gate voltages and percolation thereafter.

Key words: Zinc oxide, niobium doped zinc oxide, thin film transistors and physical characterization

[a)] Author to whom correspondence should be addressed. Electronic mail: S.Hall@liverpool.ac.uk

Zinc oxide (ZnO) has received a great deal of attention over recent years particularly for the application of transparent electronics for active matrix displays. ZnO shows advantages compared to materials such as amorphous silicon in terms of higher saturation mobilities,[1,2] and a larger band gap (Eg ~ 3.37 eV)[1] enabling the potential for transparent display technology. The atomic layer deposition (ALD) of ZnO provides the potential for large area homogeneous films. Low temperature ALD (< 150 ^{o}C) is known to achieve the best performance as the films are less conductive, with reported mobilities > 10 cm^2/Vs.[3-5] However, indium gallium zinc oxide (IGZO) is the preferred ZnO based material for thin film transistors (TFTs)[6] due to its relatively high electron mobility, stability and good control of conductivity.

However, for large scale production , non-indium based materials are desirable for cost effectiveness, hence the requirement for alternative dopants. Research into non-indium based ZnO materials for TFT application include: gallium,[7] silicon[8] and magnesium.[9] These dopants act as effective oxygen vacancy (V_o) suppressors and can further increase the band-gap of the ZnO through the Burstein-Moss effect.[7-9] Niobium (Nb) has potential as a dopant, due to its high valency (Nb^{5+}) which offers the prospect of a V_o suppressor, superior to the dopants gallium (Ga^{3+}), silicon (Si^{4+}) and magnesium (Mg^{2+}). Furthermore, Nb can act as an effective substitutional dopant for Zn^{2+} and subsequently reduce disorder and carrier scattering. To date, studies of Nb-doped ZnO (NbZnO) films have been reported using pulse layer deposition (PLD) [10,11] and sputtering.[12] The use of Nb-doping in transparent semiconducting oxides has been reported for TiO_x TFTs.[13] In this letter we present physical and electrical characteristics of NbZnO films for active layers in TFT applications.

The NbZnO films of nominal thickness 50 nm were deposited using ALD on heavily doped, thermally oxidized (50 nm) n-type Si wafers. A capping layer of 5 nm Al_2O_3 was first deposited by ALD at 200 ^{o}C on the SiO_2 The active layer NbZnO was then deposited at 200 ^{o}C using the precursors diethlyzinc (DEZn) and niobium pentaethoxide ($Nb(OEt)_5$); temperatures of these precursors entering the chamber were ambient and 140 ^{o}C respectively. The Nb ALD cycle fraction was varied from 1% to 12.5%, where the NbZnO films were made by first depositing x-cycles of ZnO by successive steps of DEZn and then H_2O vapor on the surface. After the x-cycles of ZnO, a single Nb_2O_5 cycle is deposited by successive steps of $Nb(OEt)_5$ and H_2O. The process is repeated until the desired film thickness is reached. For example, a film with a Nb cycle percentage of 2% would be achieved by 49 cycles of DEZn and H_2O (x = 49) followed by 1 cycle of $Nb(OEt)_5$ and H_2O repeated 6 times giving a total of 294

ZnO and 6 Nb_2O_5 cycles. This equates to a cycle fraction of 0.02 and cycle percentage of 2% (6/(294+6)×100%=2%). The thickness of the films was confirmed by spectroscopic ellipsometry as 52 ± 2 nm. The effect of ALD growth temperature was tested for 3.8% NbZnO at 150, 175, 200 and 225 ^{o}C.

X-ray diffraction (XRD), photoluminescence (PL) and X-ray photoelectron spectroscopy (XPS) were performed to determine the crystallographic nature, optical properties and composition respectively. The XRD measurements were performed on 1% NbZnO as-deposited, 1% to 12.5% NbZnO annealed for 1 hour at 300 ^{o}C air and 3.8% NbZnO grown at 150 ^{o}C, 200 ^{o}C and 225 ^{o}C annealed under the same conditions. The crystalline phases were identified by XRD using Cu Kα radiation (0.154051 nm, 40 kV, and 50 mA) and the diffraction patterns are shown in Figs. 1(a) and 1(b). The films are polycrystalline with peaks (100), (002) and (101). Fig. 1(a) shows the comparison between a 1% NbZnO film as-grown at 200 °C and after annealing. The act of annealing in air enhances the film crystallinity as indicated by the increase in the intensity of the (100) and (101) peaks as well as the reduction of their full width at half maxima (FWHM) from 0.50 to 0.45 and 0.51 to 0.44 respectively. In general there is greater (002) directionality, although as the Nb content is increased, the films crystallinity is reduced eventually becoming amorphous at 9.1% and above. For the (002) peak, the grain size is reduced from 20 to 14 nm from 1% to 6.8% Nb calculated using the Scherrer equation.[14] This reduction in ZnO crystallinity with Nb concentration has also been reported when grown using PLD.[11] Fig. 1(b), demonstrates that the reducing the growth temperature serves to reduce the crystallinity of the ZnO as there are no observable (002) or (101) peaks at 150 ^{o}C.

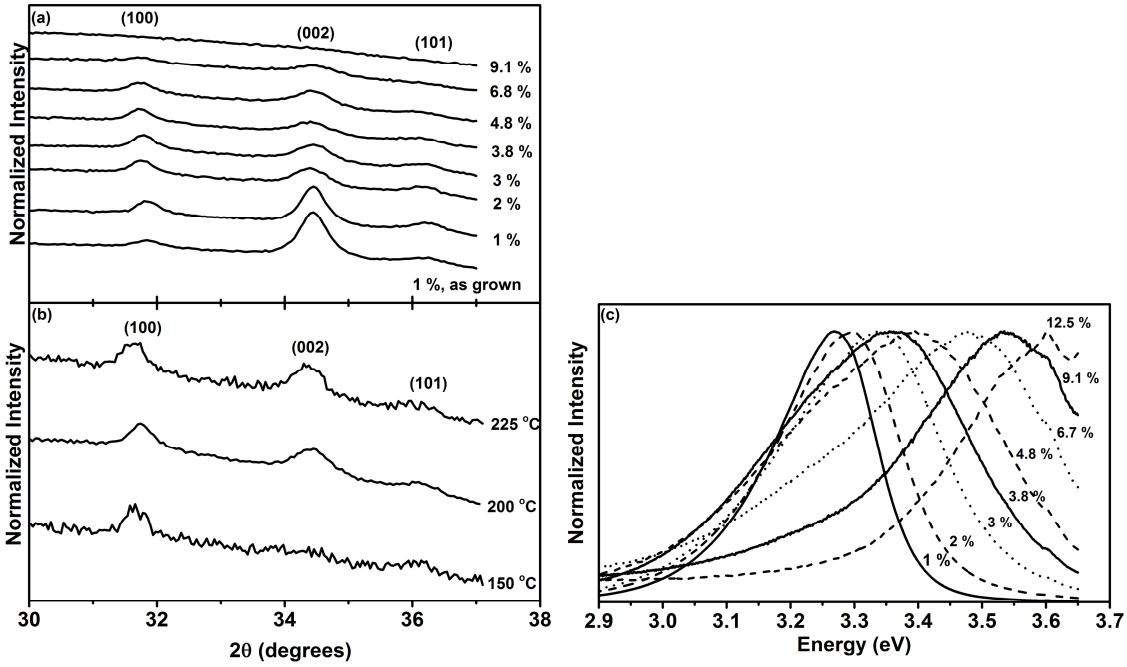

Fig. 1 Physical characterization for NbZnO films (a) XRD for different Nb cycle percentages annealed at 300 °C and 1% NbZnO as grown at 200 °C, (b) XRD of 3.8% NbZnO grown at different temperatures (c) PL of NbZnO with increasing Nb content

The PL measurements were performed using a 325 nm (3.82 eV) He-Cd laser and a Raman confocal microscope set to 100 µm aperture coupled to a single grating spectrometer equipped with a notch filter and a CCD camera detector. The PL spectrum of the as-deposited samples with varying Nb content is shown in Fig. 1(c). As the Nb cycle percentage is increased, the band edge increases to 3.58 eV, consistent with spectroscopic ellipsometry results.[15] This increase can be described by the Burstein-Moss effect; similar band energy shifts have been reported for NbZnO prepared by PLD,[11,16,17]

The core level (CL) structure and occupied density of states in the valence band were probed by XPS, further experimental details of which can be found elsewhere.[18] For the XPS measurements, 10 nm films were used, which corresponds to the nominal surface sensitivity of the technique. Core level peak energies were corrected using adventitious carbon C 1s peak at 284.6 eV for all samples. The CL spectra for the Nb $3d_{5/2}$, Zn $2p_{3/2}$, 3.8% and 12.5% NbZnO grown at 200 ^{o}C are shown in Fig. 2. Fig. 2(a) shows that the Nb $3d_{5/2}$ peak, for bulk Nb_2O_5 has a binding energy (BE) of 207.1 eV indicating the presence of Nb^{5+}.[19] For 3.8% and 12.5% NbZnO, the Nb $3d_{5/2}$ peak shifts to a lower BE of 206.8 eV. Conversely, Fig. 2(b) indicates an increase in the BE for the Zn $2p_{3/2}$ peak, from 1020.1 eV for bulk ZnO to 1021.2 eV and 1021.3 eV for 3.8% and 12.5% NbZnO respectively. This implies that

Nb^{5+} species are present in the film as a substitutional dopant due to the nature of the charge transfer. Fig. 2(c) indicates that for bulk ZnO, the O 1s CL shows 3 sub-peaks relating to (i) the oxygen atoms bonded with nearest neighbor metal ion species (Zn-O), (ii) the oxygen atoms in the vicinity of an oxygen vacancy (labelled as O^{2-} deficiency peak) and (iii) surface oxygen such as O-C-O or hydroxyl groups.[19] Furthermore, 3.8 and 12.5% NbZnO have these sub-peaks with addition of a sub-peak with a BE of 530.5 eV which we assign to the presence of an Nb-O environment confirmed by the O 1s Nb_2O_5 peak (see supplementary material). It is evident that the O 1s CL shifts to higher binding energies with the addition of Nb from 529.5 eV to 529.9 eV as a consequence of Nb^{5+} species present within the film. Furthermore, it is evident that there is an increase of O^{2-} deficiencies with increasing Nb^{5+}, shown by the increased sub-peak at 531.4 eV.[20,21] Moreover, from the XRD spectra in Fig. 1(a), increasing Nb doping concentration serves to reduce the film crystallinity, potentially creating more dangling bonds; hence, the higher ratio of O^{2-} deficiency sub-peak for 12.5% NbZnO. Subsequently, the oxygen vacancies can be reduced by annealing in an oxygen rich environment (see supplementary material). The high binding energy sub-peak likely to be due to O-C-O, experiences a slight increase with Nb content, presumably related to carbon residue from the ALD process. It is worth noting, that the percentage of Nb within the films was estimated to be 4% and 14% for the 3.8% and 12.5% NbZnO respectively, demonstrating that, for ALD NbZnO, Nb doping does not hinder the growth of the ZnO.

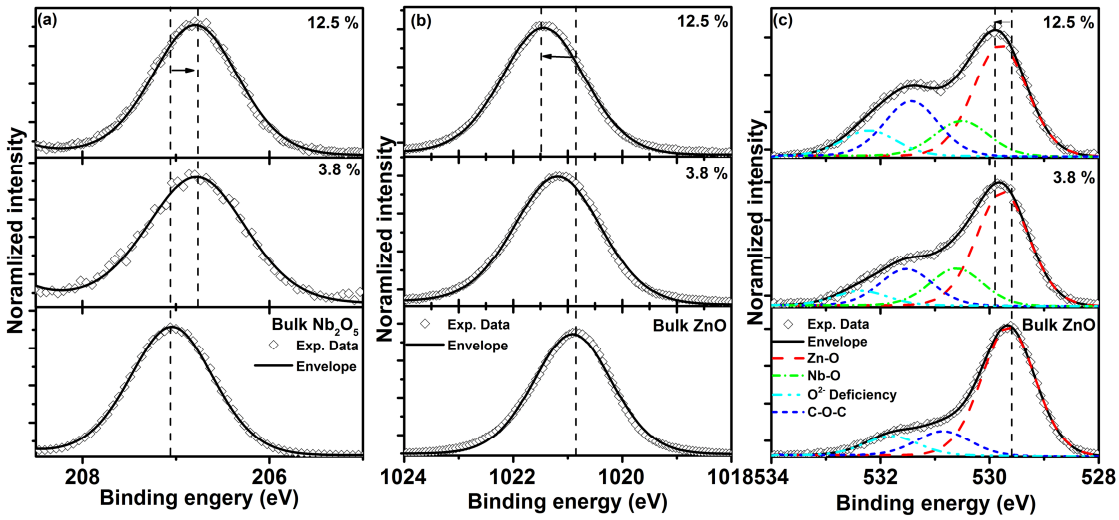

Fig. 2 XPS fittings of (a) Nb $3d_{5/2}$ core level for bulk Nb_2O_5, 3.8% NbZnO and 12.5% NbZnO (b) Zn $2p_{3/2}$ core level for bulk ZnO, 3.8% NbZnO and 12.5% NbZnO and (c) O 1s core level for bulk ZnO, 3.8% NbZnO and 12.5% NbZnO

TFTs were fabricated using 3.8% NbZnO, deposited at 150, 175, 200 and 225 ^{o}C. The aluminum source/drain contacts were thermal evaporated and patterned using photolithography. The channel length (L) and width (W) are 40 µm and 400 µm respectively. Finally the TFTs were annealed in air for 1 hour to further reduce the film conductivity. It is conventional practice to utilize the ideal MOSFET equation extract key parameters, to enable effective comparison of results in the literature: $I_{DS} = \frac{W}{2L} C_{ox} \mu_{sat} (V_{GS} - V_T)^2$ for

$V_{DS} > V_{GS} - V_T$ (1)

where C_{ox} is the gate capacitance per unit area, μ_{sat} is the effective saturation mobility, V_{GS} , V_T and V_{DS} are the gate, threshold and drain voltages respectively. The subthreshold swing (SS) is defined in the usual manner, as $\left(\log(I_{DS})/V_{GS}\right)^{-1}$.

Table I shows the extracted parameters for different growth temperatures, together with pure ZnO and 12.5 % NbZnO for the purpose of comparison. Typical TFT output and transfer characteristics are shown in Figs. 3(a) and (b) respectively for the 3.8% NbZnO film grown at 175 ^{o}C, where the symbols designate measured characteristics.

Table I. TFT characteristics for the NbZnO growth temperature study and comparison with pure ZnO and 12.5 % NbZnO showing the average of 5 measured devices

Nb cycle %	Temp. (^{o}C)	On/Off ratio	V_T (V)	μ_{sat} (cm^2/Vs)	SS (mV/dec)	V_{FB} (V)	T_o (K)
0[15]	200	1×10^4	9.3 ± 1.0	1.4 ± 0.2	2970 ± 300	-	-
3.8	150	3×10^8	7.9 ± 0.2	4.8 ± 0.1	220 ± 20	-4.0	539
	175	1×10^8	8.5 ± 0.1	7.9 ± 0.1	340 ± 40	-1.5	541
	200	1×10^7	9.3 ± 0.1	7.9 ± 0.1	470 ± 30	-3.3	570
	225	9×10^6	9.8 ± 0.1	7.0 ± 0.1	870 ± 20	-1.2	620
12.5[15]	200	1×10^7	1.0 ± 1.0	0.1 ± 0.1	1080 ± 200	-	-

Comparing the different Nb cycle percentages in Table I, it is evident that Nb serves to increase the On/Off ratio by reducing the off-current[15]. The On/Off ratio is defined as the maximum current and when the TFT begins to conduct. Moreover, small Nb cycle percentages serve to increase on-current; however, increased Nb concentration reduces the films conductivity, indicated by the change in μ_{sat}[15] The improved μ_{sat}, is considered to be due to the high oxidation state of Nb^{5+}. Table 1 indicates that the On/Off ratio decreases with increasing growth temperature for 3.8 % NbZnO, together with a positive shift in V_T. Furthermore, μ_{sat} stays about the same for temperatures above 175 ^{o}C. The lower mobility for 150 ^{o}C NbZnO can be attributed to the reduced crystallinity apparent from Fig. 1(b).

Conversely *SS* is improved for the lower temperature grown NbZnO, implying a better interface between Al_2O_3 and NbZnO. It is evident from Table I that the 175 ^oC NbZnO TFT has the best characteristics with On/Off ratio = 1 × 10^8, μ_{sat} = 7.9 cm^2/Vs and *SS* = 340 mV/dec.

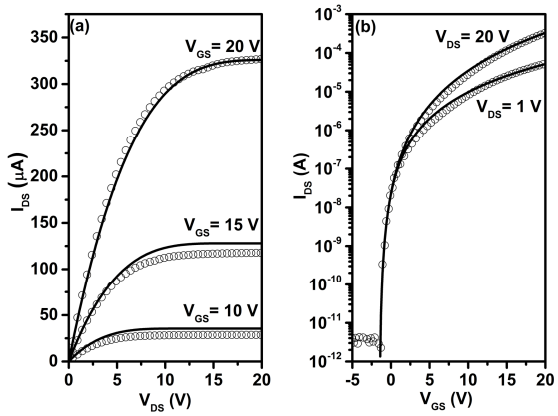

Fig. 3 (a) Output characteristics and (b) transfer characteristics for V_{DS}= 1 V and V_{DS}= 20 V of 175 ^oC grown 3.8% NbZnO TFTs. The solid line shows the fitted theory of Eqn.2.

More appropriate physical modelling of the TFTs is achieved by considering a power law dependency of current on gate voltage which arises by considering an exponential density of electron states (DoS) in the material.[22] The drain current mechanism is then described by the multi-trapping and release (MTR) model:

$$I_{DS} = \frac{W}{L}\beta\left[(V_{GS} - V_{FB} - (I_{DS}R_S)^{\gamma} - (V_{GS} - V_{FB} - (I_{DS}R_D)^{\gamma}\right] \quad (2)$$

The power law index is defined as $\gamma = T_o/T$ where T_o is a characteristic temperature related to the exponential DoS;[22] V_{FB} is the flat band voltage, β is a transconductance parameter and R_S and R_D are the source and drain series resistances respectively. Fitting of (2) with experimental data was performed by linear regression with a regression coefficient, R^2 of 0.99 and 0.93 for the transfer output characteristics respectively. Fits for the 175 ^oC NbZnO TFT are shown in Fig. 3. The power dependency of I_{DS}, increased from 3.6 to 4.13 with temperature and the corresponding T_o shown in Table I. It can be seen that T_o and *SS* are correlated and is representative of the degree of disorder in the film, which translates into a poorer *SS*. Comparing the TFT performance with our similar work on Mg doping,[23] the lower T_o and *SS* indicate that Nb is a more effective dopant for ZnO. Furthermore, it has been

reported for metal oxide semiconductors that for sufficiently large V_{GS}, a mechanism of percolation dominates the current transport.[24,25] Following the analysis outlined in, [24,25] the TFTs are seen to follow similar transport physics with the onset of percolation current ($E_F = E_C$) at $V_{GS} \approx 5$ V for 175 ^{o}C NbZnO. The associated effective density of tail states was found to be 1.5×10^{18} cm^{-3}.

In conclusion, ALD has been used to deposit NbZnO films for TFT applications. It has been established from XPS that Nb^{5+} exists within the NbZnO matrix. Furthermore, XRD indicates NbZnO films are polycrystalline with low Nb cycle percentages over a range of growth temperatures. However, as the Nb cycle percentage increases, the films become amorphous whilst shifting the band gap to higher energies. Optimum TFT performance was achieved with 175 ^{o}C 3.8% NbZnO where the μ_{sat} is superior to ALD ZnO doped with Mg[9] and Si[8]. See supplementary material for XPS CL spectra of bulk Nb_2O_5 O 1s and effects of annealing in air on 12.5 % NbZnO O 1s.

The authors thank the Engineering and Physical Sciences Research Council (EPSRC) for funding this project under Grant No: EP/K018884/1. VRD acknowledges support through the EPSRC Capital for Great Technologies - Grid Scale Energy Storage Programme; TJW acknowledges funding through the EPSRC (Grant No. EP/J500471/1); the authors thank David Hesp for help with the XPS measurements.

1 E. Fortunato, P. Barquinha, and R. Martins, Adv. Mater. 24 (22), 2945 (2012).
2 C. Brox-Nilsen, J. Jin, Y. Luo, P. Bao, and A. M. Song, IEEE Trans. Electron Devices 60 (10), 3424 (2013).
3 P. K. Nayak, Z. Wang, and H. N. Alshareef, Adv. Mater. 28 (35), 7736 (2016).
4 Y. Y. Lin, C. C. Hsu, M. H. Tseng, J. J. Shyue, and F. Y. Tsai, ACS Appl. Mater. Interfaces 7 (40), 22610 (2015).
5 Y. H. Wang, Q. Ma, L. L. Zheng, W. J. Liu, S. J. Ding, H. L. Lu, and D. W. Zhang, IEEE Trans. Electron Devices 63 (5), 1893 (2016).
6 H. Hosono, J. Non·Cryst. Solids 352, 851 (2006).
7 W. J. Park, H. S. Shin, B. D. Ahn, G. H. Kim, S. M. Lee, K. H. Kim, and H. J. Kim, Appl. Phys. Lett. 93 (8), 083508 (2008).
8 S. H. Lee, K. W. Cha, and J. S. Park, Thin Solid Films 596, 72 (2015).
9 J. S. Wrench, I. F. Brunell, P. R. Chalker, J. D. Jin, A. Shaw, I. Z. Mitrovic, and S. Hall, Appl. Phys. Lett. 105 (20), 202109 (2014).
10 J. M. Lin, Y. Z. Zhang, Z. Z. Ye, X. Q. Gu, X. H. Pan, Y. F. Yang, J. G. Lu, H. P. He, and B. H. Zhao, Appl. Surf. Sci. 255 (13–14), 6460 (2009).
11 J. Shao, W. Dong, D. Li, R. Tao, Z. Deng, T. Wang, G. Meng, S. Zhou, and X. Fang, Thin Solid Films 518 (18), 5288 (2010).
12 F. Cao, Y. D. Wang, D. L. Liu, J. Z. Yin, B. J. Guo, L. Li, and Y. P. An, Chin. Phys. Lett. 26 (3), 034210 (2009).

[13] K. C. Ok, J. Park, J. H. Lee, B. D. Ahn, J. H. Lee, K. B. Chung, and J. S. Park, Appl. Phys. Lett. 100 (14), 142103 (2012).
[14] A. L. Patterson, Phys. Rev. 56 (10), 978 (1939).
[15] A. Shaw, J. D. Jin, I. Z. Mitrovic, S. Hall, J. S. Wrench, and P. R. Chalker, in *2016 Joint International EUROSOI Workshop and International Conference on Ultimate Integration on Silicon (EUROSOI-ULIS)*, Vienna, Austria, 25-27th January 2016, (IEEE, New York, 2016), 28.
[16] V. Gokulakrishnan, S. Parthiban, K. Jeganathan, and K. Ramamurthi, J. Electron. Mater. 40 (12), 2382 (2011).
[17] Hyun Yoon, Bhavana N. Joshi, Seung-Heon Na, Jae-Young Choi, and Sam S. Yoon, Ceram. Int. 40 (5), 7567 (2014).
[18] T. J. Whittles, L. A. Burton, J. M. Skelton, A. Walsh, T. D. Veal, and V. R. Dhanak, Chem. Mater. 28 (11), 3718 (2016).
[19] M. K. Bahl, J. Phys. Chem. Solids 36 (6), 485 (1975).
[20] P. T. Hsieh, Y. C. Chen, K. S. Kao, and C. M. Wang, Appl. Phys. A 90 (2), 317 (2008).
[21] Y. Jung, W. Yang, C. Y. Koo, K. Song, and J. Moon, J. Mater. Chem. 22 (12), 5390 (2012).
[22] F. Torricelli, J. R. Meijboom, E. Smits, A. K. Tripathi, M. Ferroni, S. Federici, G. H. Gelinck, L. Colalongo, Z. M. Kovacs-Vajna, D. de Leeuw, and E. Cantatore, IEEE Trans. Electron Devices 58 (8), 2610 (2011).
[23] A. Shaw, T. J. Whittles, I. Z. Mitrovic, J. D. Jin, J. S. Wrench, D. Hesp, V. R. Dhanak, P. R. Chalker, and S. Hall, in *European Solid-State Device Research Conference*, Graz, Austria, 14-18th September, 2015, (IEEE, New York, 2015), 206.
[24] S. Lee, K. Ghaffarzadeh, A. Nathan, J. Robertson, S. Jeon, C. Kim, I. H. Song, and U. I. Chung, Appl. Phys. Lett. 98 (20), 203508 (2011).
[25] M. Ghittorelli, F. Torricelli, and Z. M. Kovács-Vajna, IEEE Electron Device Lett. 36 (12), 1340 (2015).

Supplementary Information

Atomic Layer Deposition of Nb-doped ZnO for Thin Film Transistors

A. Shaw[1], J. S. Wrench[2], J. D. Jin[1], T. J. Whittles[3], I. Z. Mitrovic[1], M. Raja[1], V. R. Dhanak[3], P.R. Chalker[2] and S. Hall[1a)]

[1] *Department of Electrical and Electronic Engineering, University of Liverpool, Liverpool, L69 3GJ, United Kingdom*

[2]*School of Engineering, Centre for Materials and Structures, University of Liverpool, Liverpool L69 3GH, United Kingdom*

[3]*Department of Physics and Stephenson Institute of Renewable Energy, University of Liverpool, Liverpool L69 3BX, United Kingdom*

Supplementary Figures

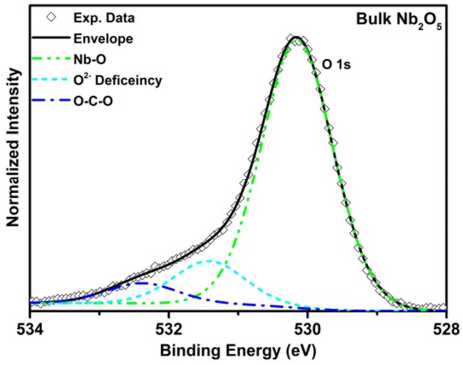

Fig. S1 XPS fittings for O 1s core level for bulk Nb_2O_5

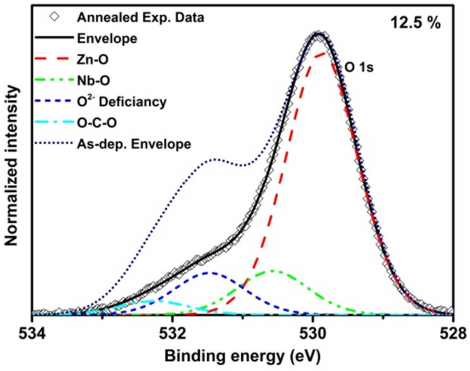

Fig. S2 Comparison of the XPS fitting for O 1s core level of 12.5 % ZnO as-deposited after annealing in air at 300 ^{o}C for 1 hour